

## An RF Energy Harvester with MPPT Operating Across a Wide Range of Available Input Power

Martins, Gustavo C.; Serdijn, Wouter A.

**DOI**

[10.1109/ISCAS.2018.8351011](https://doi.org/10.1109/ISCAS.2018.8351011)

**Publication date**

2018

**Document Version**

Accepted author manuscript

**Published in**

2018 IEEE International Symposium on Circuits and Systems, ISCAS 2018

**Citation (APA)**

Martins, G. C., & Serdijn, W. A. (2018). An RF Energy Harvester with MPPT Operating Across a Wide Range of Available Input Power. In *2018 IEEE International Symposium on Circuits and Systems, ISCAS 2018: Proceedings* (Vol. 2018-May, pp. 1-5). Article 8351011 IEEE.  
<https://doi.org/10.1109/ISCAS.2018.8351011>

**Important note**

To cite this publication, please use the final published version (if applicable).  
Please check the document version above.

**Copyright**

Other than for strictly personal use, it is not permitted to download, forward or distribute the text or part of it, without the consent of the author(s) and/or copyright holder(s), unless the work is under an open content license such as Creative Commons.

**Takedown policy**

Please contact us and provide details if you believe this document breaches copyrights.  
We will remove access to the work immediately and investigate your claim.

# An RF Energy Harvester with MPPT Operating Across a Wide Range of Available Input Power

Gustavo C. Martins and Wouter A. Serdijn

Section Bioelectronics, Delft University of Technology, Delft, The Netherlands

Email: g.martins@ieee.org, w.a.serdijn@tudelft.nl

**Abstract**—In this paper we present the design and simulation results of an RF energy harvesting circuit that operates across a wide range of available input power, from  $-27$  dBm to  $6$  dBm. The system comprises an adaptive impedance matching network, a single-stage cross-connected differential rectifier, a start-up charge pump, an adaptive buck-boost converter and a Maximum Power Point Tracking (MPPT) circuit. The MPPT circuit controls the switching frequency of the buck-boost converter and configures the impedance matching network, optimizing the interfaces between the rectifier and antenna and between the rectifier and the storage capacitor, thereby guaranteeing that maximum power is being harvested. The system is designed in a standard  $0.18 \mu\text{m}$  CMOS technology. The peak efficiency is  $49.1\%$  at an available input power of  $-18$  dBm and signal frequency of  $403.5$  MHz.

## I. INTRODUCTION

Energy harvesting (EH) is an enabling technology for powering devices that are difficult or inconvenient to access physically, such as IoT, biomedical or several industrial applications. Among the EH modalities, radio-frequency energy harvesting (RFEH) is promising due to the ubiquity of RF signals in urban environments and due to its ability to reach environments in which other sources of energy (sunlight, vibration, temperature gradients, etc.) are not present. The available power presented on the antenna terminals of the RFEH can vary due to many factors, such as antenna alignment, distance to the source and network traffic. However, RFEHs are conventionally designed to present high sensitivity and do not accommodate for such power variations. Therefore, it is possible to observe a reduction in the power conversion efficiency (PCE) once the available power increases.

In order to tackle this problem, some systems in the literature present a certain degree of reconfigurability. For example, both in [1] and [2], a reconfigurable rectifier is used. However, in both cases, the extra stages are always connected to the input and the extra capacitances reduce the input voltage amplitude, reducing the PCE [3], which is a problem especially when the available power is low. In [4], three power paths are connected in parallel: a reference path, a low-power path and a high-power path. The voltage at the output of the reference path is sensed to make the decision about using the high-power path or the low-power one. Still, the switches in the signal path introduce losses and when the low-power path is activated the high-power one is also connected to the antenna terminals, which increases the parasitic capacitance.

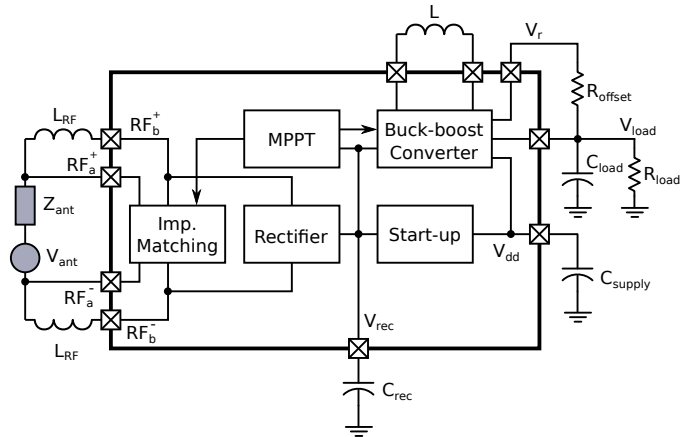


Fig. 1. System block diagram

In this work, we employ a single-stage cross-connected differential rectifier to perform the RF-DC conversion and we design the impedance matching circuit and a DC-DC converter to be configurable in order to adapt for the input power variation. The system architecture and specific circuit schematics are presented in the next section. In Section III, the post-layout simulation results are presented. In Section IV, the concluding remarks are discussed.

## II. SYSTEM DESCRIPTION

The system block diagram is presented in Fig. 1. The goal of the system is to convert the RF power received by the antenna into DC power delivered to  $R_{load}$ . The impedance matching network performs a conjugated match of the antenna impedance to the rectifier input impedance, in order to maximize the power transfer from the antenna to the rectifier. To convert the RF signal into DC, a cross-connected differential rectifier is used [5]. A buck-boost DC-DC converter up-converts the rectifier output voltage to supply  $R_{load}$ . Because the rectifier input impedance and optimum output load change with the available power  $P_{av}$  presented to the antenna, we employ a Maximum Power Point Tracking (MPPT) circuit to configure the impedance matching and the buck-boost converter. A charge pump that can operate with a low supply voltage starts the system up by initially charging  $C_{supply}$ . The buck-boost converter control circuitry draws energy from  $C_{supply}$  to operate. One of the outputs of the converter is



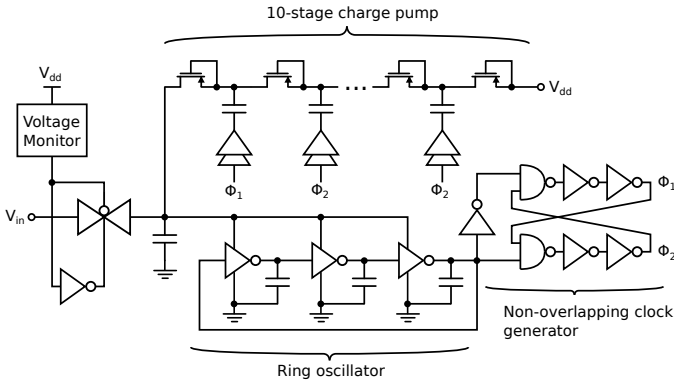


Fig. 5. Start-up circuit diagram.

switching period  $T_s$  and is given by:

$$R_{in,avg} = \frac{V_{in}}{I_{in,avg}} = \frac{2L}{D^2 T_s}, \quad (1)$$

in which  $D$  is the duty cycle of the switching control signal ( $DT$  is the ON-time of the converter) and  $L$  is the inductor value. The inductor used is a  $220 \mu\text{H}$  inductor with a maximum parasitic series DC resistance of  $21.1 \Omega$  (Coilcraft XPL2010-224ML). The switching frequency  $f_s$  is controlled by the MPPT, which outputs a 9-bit control signal along a thermometric scale. This control signal is used to control the bias current that drives the relaxation oscillator, whose frequency ranges from  $10 \text{ kHz}$  to  $1 \text{ MHz}$ .

The current necessary for the operation of the converter is drawn from  $C_{supply}$ . This capacitor is recharged by the buck-boost converter itself, through switch  $S_5$ . A voltage monitor checks if  $V_{dd}$  is below  $1.8 \text{ V}$  and, if this is the case, the next current pulse is directed to  $C_{supply}$ . The configurable switch technique is not applied to this switch, since it is operating sporadically (as most of the power is directed to the load). This avoids an unnecessary increment of parasitic capacitance, which degrades the efficiency.

### C. Start-up Charge Pump

The buck-boost converter can operate from  $V_{dd} > 1.1 \text{ V}$ . If this condition is met, it can charge  $C_{supply}$  until its voltage reaches  $1.8 \text{ V}$ . To charge  $C_{supply}$  up to  $1.1 \text{ V}$ , the start-up circuit presented in Fig. 5 is used. It comprises a charge pump with 10 stages (which provides a 9x multiplication of the input voltage, ideally), a ring oscillator and a non-overlapping clock generator. It is supplied by the rectifier output  $V_{rec}$ , the same node it draws energy from to charge  $C_{supply}$ . After the start-up is complete, this circuit is turned off and it is activated only if  $V_{dd}$  becomes too low. Simulation results show that it can start-up the system with  $V_{rec}$  as low as  $300 \text{ mV}$ .

### D. Maximum Power Point Tracking

The hill climbing algorithm is used since it is a low-power MPPT algorithm, due to its simplicity [8]. The block diagram of the MPPT is shown in Fig. 6. It consists of estimating the input power  $P_{in}$  of the buck-boost converter, holding this

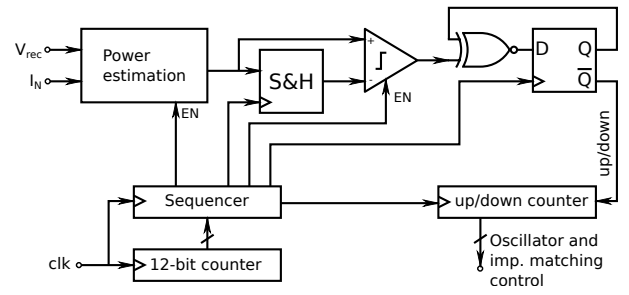


Fig. 6. MPPT block diagram.

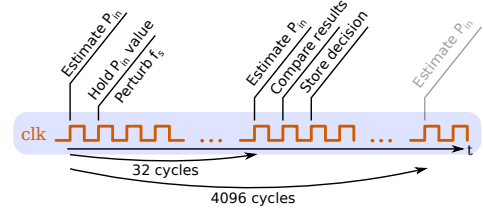


Fig. 7. Timing diagram of the MPPT circuit.

value, changing  $f_s$  and comparing the new  $P_{in}$  value to the previous one. In case the new  $P_{in}$  is higher, the frequency is further increased. Otherwise, the frequency is decreased. This is done by activating the up-down counter, which controls the oscillator frequency (by controlling its bias current  $I_N$ ). When the counter value is higher than a certain threshold,  $V_{hp}$  is high, signaling the presence of a high input power to the other blocks.

If the MPPT cycle is performed frequently, the average power consumption of the MPPT will be high. However, power is wasted to hold the input power value for a long period, since the holding circuit cannot be switched off between estimations. To overcome this problem, the sequence presented in Fig. 7 is proposed. The MPPT cycle begins with estimating  $P_{in}$ . The perturbation is performed (either increasing or decreasing the switching frequency) and the current value of  $P_{in}$  is held for just enough time for  $V_{rec}$  to settle. Subsequently, the new estimation and the comparison are done. The result of this comparison is held on a flip-flop, which does not dissipate static power, except for leakage. This cycle is continuously repeated during the operation of the energy harvester. The power consumption of the MPPT is  $17.4 \text{ nW}$  for  $f_s = 20 \text{ kHz}$ , for which  $P_{in}$  is nominally equal to  $1 \mu\text{W}$  (at  $V_{rec} = 0.38 \text{ V}$ ).

## III. SIMULATION RESULTS

The system described in this paper was designed in AMS  $0.18 \mu\text{m}$  CMOS technology. The chip layout is shown in Fig. 8. Its active area is less than  $0.2 \text{ mm}^2$ . The results presented here are post-layout simulation results.

To perform the system simulations, we apply a  $403.5 \text{ MHz}$  differential signal at the harvester input and place a resistive load  $R_{load}$  in parallel with  $C_{load}$  at its output. The value of  $R_{load}$  is selected so that  $V_{load} = 1.8 \text{ V}$  in steady state. Therefore, a different  $R_{load}$  is selected when applying a

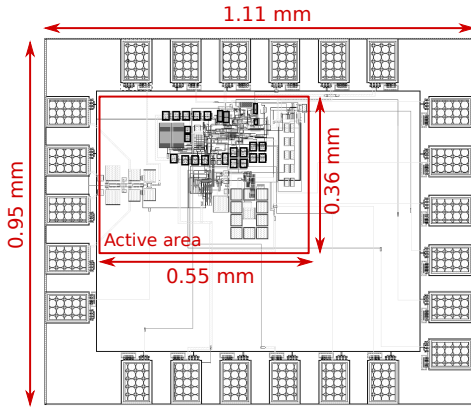


Fig. 8. Chip layout.

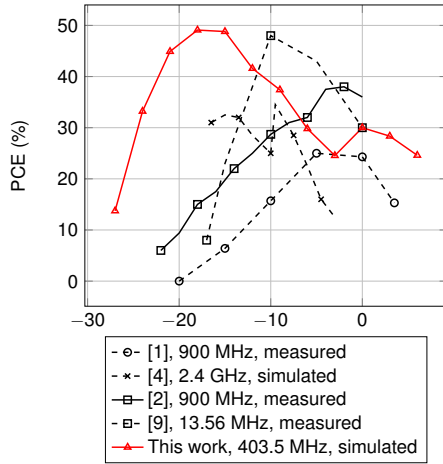


Fig. 9. Power conversion efficiency versus available input power for state-of-the-art RF energy harvesters.

different  $P_{av}$ . In Fig. 9, the PCE is presented for a varying  $P_{av}$ , also in comparison with other state-of-the-art works. The peak efficiency is 49.1% at  $P_{av} = -18$  dBm.

In Fig. 10a, we present the  $S_{11}$  variations as a function of the RF input frequency. Since the rectifier input impedance changes with  $P_{av}$ , the bandwidth and reflection coefficient change as well. The variation of the  $S_{11}$  with  $P_{av}$ , as well as the RF-DC conversion efficiency, are presented in Fig. 10b. As can be seen, the  $S_{11}$  decreases with  $P_{av}$ , when  $P_{av}$  is between  $-18$  and  $-3$  dBm. However, when higher available power is detected (around  $P_{av} = -3$  dBm), the MPPT activates the high-power mode of the adaptive impedance matching block, decreasing the  $S_{11}$ . This results in an RF-DC conversion efficiency ( $PCE_{RF-DC}$ ) increase for  $P_{av} > -3$  dBm, extending the operating power range of the RFEH. The  $PCE_{RF-DC}$  in the high-power configuration is not as high as in the low-power configuration because the rectifier is not optimized for high power levels and because there are more losses in the implemented high-power impedance matching network compared to the low-power one.

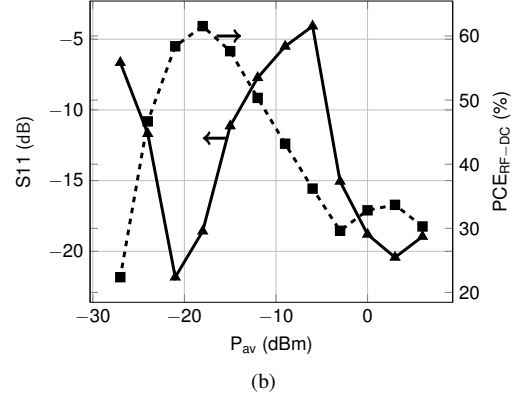
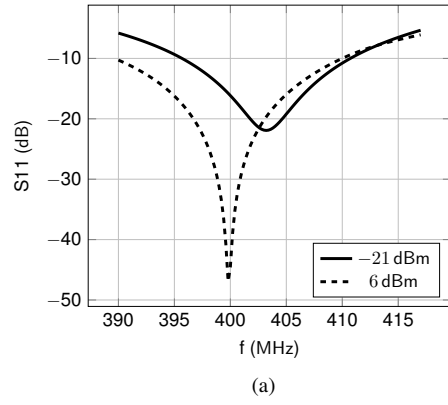


Fig. 10. Harvester  $S_{11}$  variation with (a) frequency and (b) available power.

#### IV. CONCLUSION

We have presented the circuit design and simulation results of an RFEH circuit that presents a competitive peak efficiency while operating across a wide range of available input power, of more than 3 decades. To achieve this, we employ adaptive techniques to the impedance matching and buck-boost converter blocks. Other techniques such as the adaptively-biased comparator, the configurable switches and the minimal input power estimator allow for a reduction of the power consumption when  $P_{av}$  is low and an increased power conversion efficiency for the specified  $P_{av}$  range. The antenna-rectifier and rectifier-load interfaces are controlled by the MPPT in order to accommodate for the changing input power. Simulation results show the system can operate for available input powers that range from  $-27$  dBm to 6 dBm. Its peak efficiency is 49.1% at  $P_{av} = -18$  dBm and  $f = 403.5$  MHz.

#### ACKNOWLEDGMENT

This work was supported by the CAPES Foundation, Brazil.

#### REFERENCES

- [1] M. A. Abouzied, K. Ravichandran, and E. Sanchez-Sinencio, "A fully integrated reconfigurable self-startup RF energy-harvesting system with storage capability," *IEEE J. Solid-State Circuits*, vol. 52, no. 3, pp. 704–719, March 2017.
- [2] Z. Zeng *et al.*, "A WLAN 2.4-GHz RF energy harvesting system with reconfigurable rectifier for wireless sensor network," in *2016 IEEE International Symposium on Circuits and Systems (ISCAS)*, May 2016, pp. 2362–2365.

- [3] M. Stoopman *et al.*, "Co-design of a CMOS rectifier and small loop antenna for highly sensitive RF energy harvesters," *IEEE J. Solid-State Circuits*, vol. 49, no. 3, pp. 622–634, March 2014.
- [4] Y. Lu *et al.*, "A wide input range dual-path CMOS rectifier for rf energy harvesting," *IEEE Trans. Circuits and Systems II: Express Briefs*, vol. 64, no. 2, pp. 166–170, Feb 2017.
- [5] K. Kotani, A. Sasaki, and T. Ito, "High-efficiency differential-drive CMOS rectifier," *IEEE J. Solid-State Circuits*, vol. 44, no. 11, pp. 3011–3018, 2009.
- [6] H. J. Visser and R. J. M. Vullers, "Rf energy harvesting and transport for wireless sensor network applications: Principles and requirements," *Proceedings of the IEEE*, vol. 101, no. 6, pp. 1410–1423, June 2013.
- [7] G. C. Martins and W. A. Serdijn, "Adaptive buck-boost converter for RF energy harvesting and transfer in biomedical applications," in *2016 Biomedical Circuits and Systems Conf. (BioCAS)*. IEEE, Oct. 2016.
- [8] W. Xiao and W. G. Dunford, "A modified adaptive hill climbing mppt method for photovoltaic power systems," in *2004 IEEE 35th Annual Power Electronics Specialists Conf.*, vol. 3, June 2004, pp. 1957–1963 Vol.3.
- [9] J. Walk *et al.*, "Remote powered medical implants for telemonitoring," *Proceedings of the IEEE*, vol. 102, no. 11, pp. 1811–1832, Nov 2014.